Title

Two-dimensional infrared spectroscopy of vibrational polaritons

Journal

Proceedings of the National Academy of Sciences of the United States of America, 115(19)

ISSN

0027-8424

Authors

Xiang, Bo
Ribeiro, Raphael F
Dunkelberger, Adam D
et al.

Publication Date

2018-05-08

DOI

10.1073/pnas.1722063115

Peer reviewed

Two-dimensional infrared spectroscopy of vibrational polaritons

Bo Xiang[a], Raphael F. Ribeiro[b], Adam D. Dunkelberger[c], Jiaxi Wang[b], Yingmin Li[a], Blake S. Simpkins[c], Jeffrey C. Owrutsky[c], Joel Yuen-Zhou[b], and Wei Xiong[a,b,1]

[a]Materials Science and Engineering Program, University of California, San Diego, La Jolla, CA 92093; [b]Department of Chemistry and Biochemistry, University of California, San Diego, La Jolla, CA 92093; and [c]Chemistry Division, Naval Research Laboratory, Washington, DC 20375

Edited by Stephen R. Forrest, University of Michigan, Ann Arbor, MI, and approved March 28, 2018 (received for review December 19, 2017)

We report experimental 2D infrared (2D IR) spectra of coherent light–matter excitations—molecular vibrational polaritons. The application of advanced 2D IR spectroscopy to vibrational polaritons challenges and advances our understanding in both fields. First, the 2D IR spectra of polaritons differ drastically from free uncoupled excitations and a new interpretation is needed. Second, 2D IR uniquely resolves excitation of hybrid light–matter polaritons and unexpected dark states in a state-selective manner, revealing otherwise hidden interactions between them. Moreover, 2D IR signals highlight the impact of molecular anharmonicities which are applicable to virtually all molecular systems. A quantum-mechanical model is developed which incorporates both nuclear and electrical anharmonicities and provides the basis for interpreting this class of 2D IR spectra. This work lays the foundation for investigating phenomena of nonlinear photonics and chemistry of molecular vibrational polaritons which cannot be probed with traditional linear spectroscopy.

vibrational polariton | two-dimensional infrared spectroscopy | ultrafast dynamics | strong coupling | microcavity

Molecular vibrational polaritons can be described as delocalized quantum superpositions of molecular vibrations and electromagnetic modes, resulting from strong coupling between them (1–3), which extend across a macroscopic number of molecules in the entire photonic mode (Fig. 1 *A* and *B*). Following the impressive developments in the field of exciton–polaritons, including room-temperature tabletop realizations of superfluids (4), polariton lasing (5), and Bose–Einstein condensates (6–9), it is anticipated that vibrational polaritons will open opportunities for new photonic and molecular phenomena. While some have been recently explored, such as chemical reactivity control through modified vibrational dynamics, and tailored potential energy landscapes (1, 2, 10–14), other promising applications are still waiting for experimental demonstrations, e.g., long-range mesoscopic vibrational energy transfer and novel optical switches and lasing in the mid-IR regime. Vibrational polaritons have been probed in polymers, neat liquids, and solutions (1, 2, 10, 12) using steady-state optical responses, including linear IR and Raman spectroscopy. This research revealed enhanced Raman scattering (11) and modified kinetics of chemical reactions, even in the absence of external pumping (2, 3, 15). The first time-resolved spectroscopic study of these systems showed vibrational-polariton dynamics that were significantly faster than that of the uncoupled molecule and highly sensitive to the light–matter composition of the polaritons (i.e., the Hopfield coefficients) (16).

However, important aspects of vibrational polaritons are still not understood because molecular vibrations behave qualitatively different from the well-studied excitons (excitons consist of an electron–hole pair while the vibrational degree of freedom is a weakly perturbed harmonic oscillator), and the polariton–polariton interactions, as well as the couplings between polaritons and other degrees of freedom, cannot be accessed through steady-state spectroscopy. For instance, it is known that the hybrid molecular-cavity system has many dark states in comparison with the few bright modes (3, 17, 18): One type of dark states shares molecular components and some small photonic character with polaritons as a result of disorder (17). Another type of dark states, termed "uncoupled" molecules, consists of molecular vibrations which are not coupled to the cavity electric field (e.g., because they may be outside the photonic-mode volume, or because their transition dipole moment is orthogonal to the mode polarization). These "uncoupled" dark states should not contribute to polariton transmission spectra. Further development of molecular vibrational-polariton photonic devices hinges on detailed understanding of the role of dark states in microcavities and how they interact with the bright polariton states. However, since dark states are essentially invisible in linear spectroscopy, we do not have very direct measurements of them as of present.

In the following, we report ultrafast 2D IR spectroscopy (19) investigation of vibrational polaritons to resolve state-selective excitation and population transfer, and thereby reveal hidden dark states and their influences on polaritons. The combined effort in utilizing 2D IR spectroscopy to study vibrational-polariton states advances our understanding of both fields. Two-dimensional IR spectroscopy can explicitly excite and detect transitions in a state-selective manner, which reveals unexpected interactions between dark states and vibrational polaritons as well as direct excitation of dark states. These vibrational polaritons bring 2D IR into an unexplored regime and present theoretical challenges. The mere existence of vibrational-polariton pump–probe (16) and 2D IR signals is direct evidence of

Significance

Quantum states of molecular vibrational polaritons, hybrid half-light, half-matter quasi-particles, are studied using ultrafast coherent two-dimensional infrared spectroscopy. Valuable physical insights such as existence of hidden dark states and ultrafast interactions between dark states and bright polariton states are unambiguously revealed. These results not only advance coherent two-dimensional spectroscopy, but also have significant implications in harvesting the creation of molecular vibrational polaritons for infrared photonic devices, lasing, molecular quantum simulation, as well as chemistry by tailoring potential energy landscapes.

Author contributions: B.X., A.D.D., J.W., Y.L., and W.X. designed research; B.X., A.D.D., J.W., Y.L., and W.X. performed research; B.X., R.F.R., A.D.D., B.S.S., J.C.O., J.Y.-Z., and W.X. analyzed data; R.F.R., A.D.D., B.S.S., J.C.O., J.Y.-Z., and W.X. developed the theoretical model; and B.X., R.F.R., A.D.D., B.S.S., J.C.O., J.Y.-Z., and W.X. wrote the paper.

The authors declare no conflict of interest.

This article is a PNAS Direct Submission.

[1]To whom correspondence should be addressed. Email: w2xiong@ucsd.edu.

This article contains supporting information online at www.pnas.org/lookup/suppl/doi:10.1073/pnas.1722063115/-/DCSupplemental.

Published online April 19, 2018.

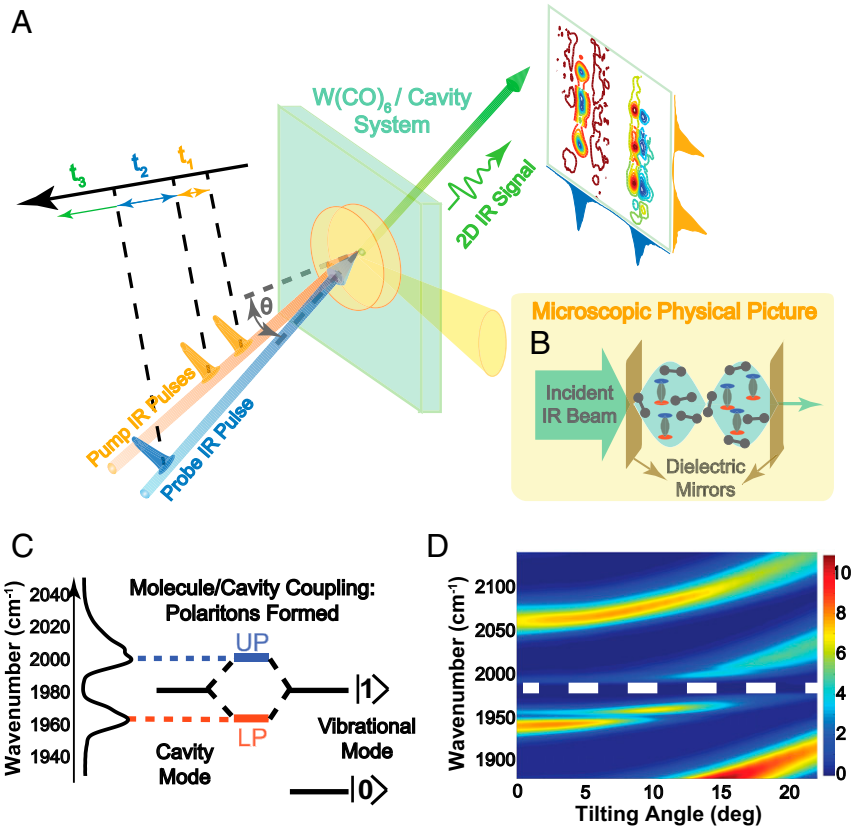

Fig. 1. Vibrational polariton 2D IR spectroscopy. (*A*) Scheme of vibrational polariton 2D IR spectroscopy setup. Pump and probe IR incident beams are symmetric with respect to the normal plane with the same tilting angle, θ. The coherences are characterized by scanning t_1 and t_3, and the resulting time-domain interferograms are Fourier transformed to obtain 2D IR spectra. The other delay time, t_2, is equivalent to the delay between the pump and probe pulses in pump–probe spectroscopy. (*B*) Illustration of the microscopic physics of molecules inside of a microcavity where "pure gray modes" correspond to the vibrational modes that are not strongly coupled to the cavity and the rest refers to the strongly coupled modes that contribute to UP (blue), LP (red), and dark reservoir modes (gray) formation. (*C*) Formation of vibrational polaritons by strongly coupled molecular vibration and cavity modes. (*Left*) vibrational polariton FTIR spectrum of $W(CO)_6$. (*D*) Dispersion of IR transmission, as a function of the tilting angle, θ, of a microcavity filled with a nearly saturated $W(CO)_6$ in hexane solution, with white dashed line indicating the vibrational frequency of $W(CO)_6$.

deviations from the harmonic polariton model and motivates our development of a theoretical treatment of nonlinear polariton response incorporating vibrational anharmonicities. We find that in contrast to the well-studied exciton polaritons, whose main source of nonlinearities is the so-called "phase-space filling" effect which arises due to Pauli exclusion (20, 21), vibrational polaritons feature different sources of nonlinearity—nuclear and electrical anharmonicities—which enable and determine optical features in the 2D IR spectra of vibrational polaritons. These findings represent a major step forward in the critical development of mid-IR sources of photonic nonlinearities.

Results

The sample is composed of a nearly saturated $W(CO)_6$ solution in a microcavity consisting of two dielectric stack mirrors separated by a 25-μm spacer (*Methods*). In the strong coupling regime, upper and lower polariton branches (termed UP and LP, respectively) are formed upon hybridization of vibrational and cavity modes (Fig. 1*C*). By adjusting the tilt angle, θ (Fig. 1*A*), the cavity resonance can be tuned across the vibrational transition, thus revealing a dispersive anticrossing and allowing control of the polariton light–matter composition (Fig. 1*D*) (1, 3, 9, 10, 12). When the cavity-vibration detuning is zero (i.e., frequency of both is 1,983 cm^{-1}), LP and UP have equal photonic and delocalized-vibration characters (Fig. 1*C*). The energy difference between the polariton branches at this condition (~37 cm^{-1}) corresponds to the vacuum Rabi splitting. Blue tuning the cavity probes an LP transition with stronger vibrational character while the UP has a higher photonic component. Red tuning has the opposite effect.

Pump–Probe and Free-Induction Decay. We first confirm that the pump–probe response of molecules both inside and outside the cavity agrees with published results (16, 22, 23). The transient spectrum for uncoupled $W(CO)_6$ (Fig. 2*A*) is well-understood. The negative feature at 1,983 cm^{-1} corresponds to ground-state bleach and stimulated emission while positive features indicate absorption in newly populated excited states. Importantly, for this uncoupled system, only the peak amplitudes vary with excited-state population, i.e., the spectral position of each transient feature remains fixed at the frequency corresponding to the excited or bleached state irrespective of the pump-induced transient population. Notable qualitative differences are observed between the bare molecule pump–probe response (Fig. 2*A*) and that of the strongly coupled system (Fig. 2*B*). As further explained below, the distinctive features in the polaritonic spectra do not necessarily correspond to transient population changes of states. Instead, they are due to the interaction of cavity photons with the matter polarization originating from excited-state absorption, ground-state bleach, and stimulated emission of reservoir modes.

To obtain 2D IR spectra, t_1 is scanned to measure the free-induction decay (FID) of vibrational coherences (*SI Appendix*, section 2f). A comparison of FID of the ω_{01} peak of $W(CO)_6$ in

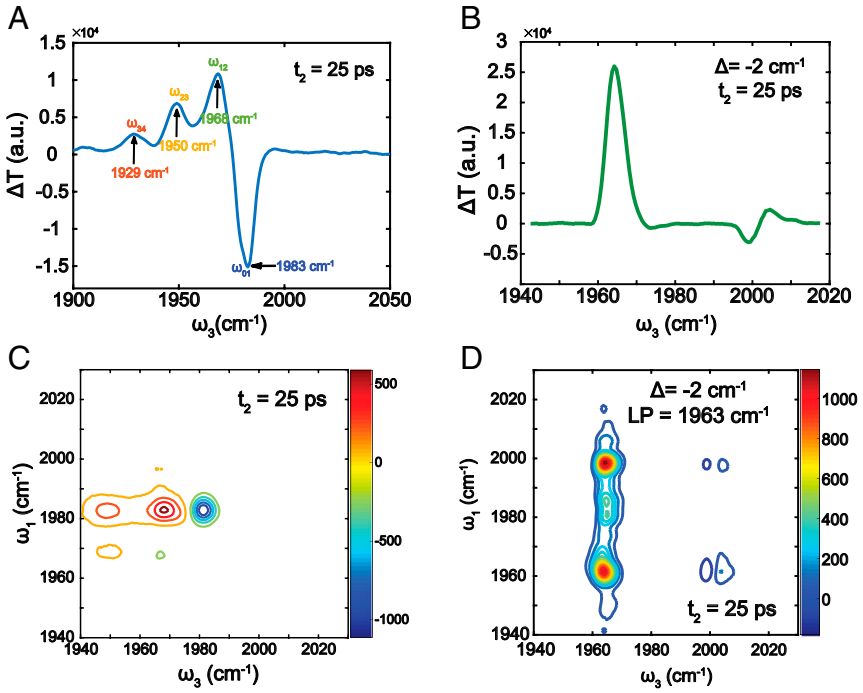

Fig. 2. Pump–probe spectra of (*A*) $W(CO)_6$ outside of the cavity. (*B*) $W(CO)_6$/cavity–vibrational polariton system with IR cavity mode detuning (Δ) of -2 cm^{-1}. By setting $t_1 = 0$, we can collect traditional pump–probe spectra. (*C*) Two-dimensional IR spectra of $W(CO)_6$ outside of cavity. (*D*) Two-dimensional IR spectra of $W(CO)_6$/cavity polariton system with IR cavity mode detuning of -2 cm^{-1}. Two-dimensional IR spectra are plotted against ω_1 (the excitation frequency) and ω_3 (the probe frequency), the coherence frequencies during t_1 and t_3, respectively, and with $t_2 = 25$ ps.

free space and the peak at 1,968 cm^{-1} in the microcavity (*SI Appendix*, Fig. S5) shows that dephasing time of the vibrational polariton is shorter than that of free-molecular vibrations for all k values. This is due to the hybrid nature of the polaritons, whose dephasing times will have a contribution from the cavity, which has shorter dephasing time than the molecule in our system. If a cavity with a narrow resonance linewidth and a long dephasing time is used, and the polariton has a large fractional photon character, we expect that dephasing times could become longer than the natural dephasing time of the vibrations of the free molecules, which has the potential to engineer long-lived coherences. Aside from the modified FID, we also observed "quantum beating." This is expected for polariton spectroscopy, since we coherently excite both UP and LP and the beating period ∼0.75 ps matches the Rabi splitting frequency. However, as we show later, unexpected "dark mode" transitions also contribute to the beating in FID traces.

Two-Dimensional IR Spectra of Vibrational Polaritons. A 2D IR spectrum is generated by numerically Fourier transforming the t_1 FID traces at individual ω_3 frequency. Two-dimensional IR spectroscopy reveals coherences between states using a three-IR-pulse sequence (Fig. 1*A*). We focus on results obtained at $t_2 =$ 25 ps, where spectral oscillations have ceased, and after which only incoherent polariton–polariton and polariton–dark-state interactions are significant. There are sharp contrasts between the 2D IR spectra of uncoupled $W(CO)_6$ (Fig. 2*C* shows ground-state bleach/stimulated emission and excited-state absorption at the frequencies of those transitions) and cavity-coupled $W(CO)_6$ (Fig. 2*D* shows strong excited-state absorption features extending along the ω_1 axis and weaker features near the UP region). We have eliminated the possibility of a cavity-induced spectral filtering effect contributing to the 2D IR spectra (*SI Appendix*, section 2g).

Details of the cavity-coupled response are more clearly seen in Fig. 3 where we have rescaled each region for visibility. Fig. 3 shows many features along the diagonal, where the system is pumped and probed at the same frequency, as well as cross-peaks, indicating coupling or energy transfer between modes. Along the diagonal, we observe a large absorptive feature in the LP region ($\omega_1 = \omega_3 = \omega_{LP}$) (Fig. 3*C*), and a derivative-like modulation in the UP region ($\omega_1 = \omega_3 = \omega_{UP}$) (Fig. 3*D*). Additionally, "cross-peaks" appear when exciting either polariton mode (24). Specifically, when the UP is excited, a strong feature (Fig. 3*A*) identical to that of Fig. 3*C* is observed when the system is probed at the LP frequency ($\omega_1 = \omega_{UP}$, $\omega_3 = \omega_{LP}$), and the derivative lineshape observed in Fig. 3*D* also appears when the LP is excited ($\omega_1 = \omega_{LP}$, $\omega_3 = \omega_{UP}$) (Fig. 3*F*). Calculations based on Fresnel expressions (16) (also see *SI Appendix*, section 3) associate the large, absorptive feature located at the LP region (∼1,960 cm^{-1}) with the coupling of the cavity mode to v = 1–2 polarization (due to transient v = 1 dark population). The derivative lineshape in the UP region and weak negative responses at the edges of the LP region are essentially manifestations of a redshift of the UP transition and a blueshift of the LP, ascribed mainly to an effective Rabi splitting contraction induced by reduction of ground-state (v = 0) population. The motion of the LP is somewhat obscured because of the large absorptive feature at the LP region. Below, a microscopic quantum-mechanical model will be presented which supports these interpretations (also see *SI Appendix*, section 4).

Unexpected 2D IR peaks reveal dark-state populations. A third set of features requires discussion. When the system is excited at the ω_{01} frequency, and probed at the LP and UP frequencies, (Fig. 3 *B* and *E*), peaks are observed, consistent with the presence of v = 1 dark-state population. While these features are similar to those discussed above, their presence when exciting at the ω_{01} frequency indicates direct excitation of dark states of $W(CO)_6$ despite their "dark" nature. This direct excitation of dark modes is

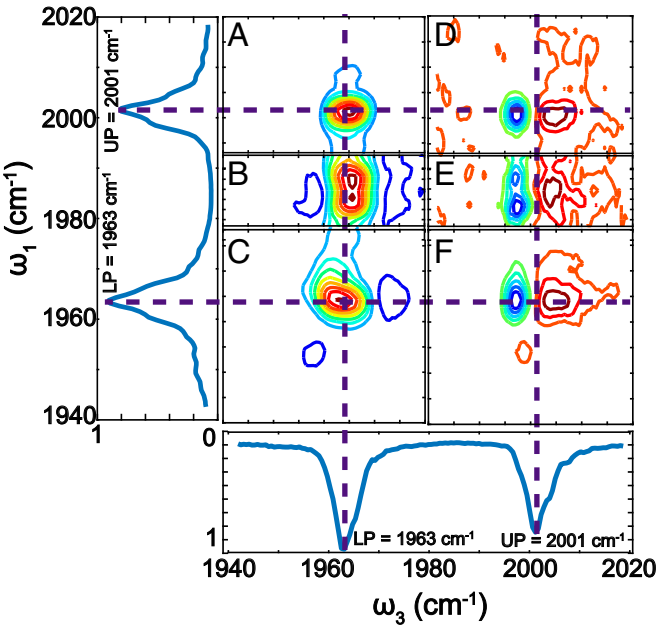

Fig. 3. Two-dimensional IR spectrum of $W(CO)_6$/cavity–polariton system at 25-ps delay with −2-cm^{-1} detuning. Each spectral region is scaled to its own intensity maximum and minimum. Spectra of the pump (ω_1) and probe (ω_3) pulses are shown on their respective axes. Color map: red is positive, blue is negative.

comparatively weak (see unscaled data of Fig. 2*D*). We believe it occurs by way of nonunity cavity reflections and disorder in the molecular system (17) [the phenomenon is analogous to the observed direct excitation of bare excitons in systems with exciton–polaritons (20)]. The former is necessary for excitation of molecular vibrations which are weakly coupled to the cavity mode, and the latter is needed for exciting dark states which share molecular components with polaritons. Given that the uncoupled molecules are not expected to have influence on polariton optical response (since they provide no contribution to the polariton states and do not affect the Rabi splitting), the correlations between vibrational polaritons and dark states (Figs. 2*D* and 3 *B* and *E*) indicate that many of the dark modes excited at 1,983 cm^{-1} are formed from molecules which contribute significantly to polariton transitions. These dark states define a coupled reservoir. Notably, disorder of the molecular system is expected to substantially localize these modes (25). Thus, we expect them to behave very similarly to pure molecule excitations—their optical transitions and lifetimes are similar to those of uncoupled molecules (16).

The features in Fig. 3 *B* and *E* have not been observed in any polariton coherent 2D spectroscopy and indicate significant interaction between the so-called dark modes and bright polaritons—when one mode (dark) is excited, it influences the optical response of the others (polaritons) (21). A similar interaction, but in the opposite order (exciting polaritons and influencing dark modes), is also evident in the 2D IR spectra. The large absorptive features in Fig. 3 *A* and *C* are due to dark-excited-state population and occur after selective excitation of either polariton. The fact that response is qualitatively similar when exciting at the LP, UP, or even the dark-state frequency indicates that there are polariton–dark-state interactions that lead polaritonic excitations (either LP or UP) to transfer into dark states possibly via phonon scattering (26, 27).

The existence of dark-state peaks imposes difficulty in disentangling certain spectral signatures. In principle, the large positive signals observed near the LP (Fig. 3 *A*–*C*) are a mixture of two contributions: nonlinear polariton optical response and excited-state absorption from the coupled reservoir-state hot bands (16). In contrast, the 2D spectra that probe UP states are easier to understand (Fig. 3 *D*–*F*), and reveal interactions between various states. For example, the derivative-like feature in Fig. 3 *E* and *F* indicates that by populating either the LP or dark modes, the UP frequency is modulated. Such insights are obfuscated when probing near the LP due to its near-resonance with the coupled reservoir excited-state absorption.

Cavity-detuning–dependent response. Important insights arise from examining the system response as a function of cavity detuning. The data in Fig. 4 correspond to spectral cuts along the probe frequency axis (ω_3) with the pump frequency (ω_1) fixed at the reservoir mode (ω_{01}), LP, and UP frequencies (ω_{LP} and ω_{UP}) (Fig. 4 *A*–*C*, respectively). The cavity is detuned by rotating the sample as described in Fig. 1*A*. When exciting at ω_1 = 1,983 cm^{-1} (dark state, Fig. 4*A*), a large positive feature is seen near the LP region; it is maximal when the cavity is tuned such that the LP frequency is 1,968 cm^{-1}. On the other hand, while the spectral cuts at LP and UP frequencies (Fig. 4 *B* and *C*) show a similar feature, it is maximized when LP is tuned to 1,963 cm^{-1}.

As discussed above, the large feature in the LP region can be attributed to the existence of an excited-state population in the v_1 coupled reservoir states. Therefore, the detuning-dependent intensity of this peak indicates either (*i*) a varying sensitivity to reservoir-state population or (*ii*) a detuning-dependent efficiency in generating coupled reservoir population. First, we examine Fig. 4*A*, where reservoir states are excited directly. In this case, the signal is maximized when the LP resonance is tuned to the ω_{12} band (~1,968 cm^{-1}). This behavior is analogous to a cavity-enhanced optical response where the excited-state population of reservoir states is most sensitively detected when the polariton resonance is coincident with the transition being probed (28, 29). In other words, the reservoir population may not be influenced much by tuning but our ability to see it is. However, when exciting the polaritons (Fig. 4 *B* and *C*), this feature is maximized when the LP frequency is 1,963 cm^{-1}. This frequency does not align with the reservoir ω_{12} transition, but it is near the condition of zero detuning between the cavity and the vibration. Under these excitation conditions, polaritons are first excited and then decay into the coupled reservoir states causing the nonlinear optical response near the LP. We propose that the generation of polariton excitations, which subsequently decay into reservoir population, is maximized when the initial polariton absorption is maximized (i.e., at zero detuning; *SI Appendix*, section 3). We note that the calculation of cavity detuning is highly sensitive to the calibration of the spectrograph and the current values are determined based on both frequencies and intensities of the LP and UP. Nevertheless, these results indicate that even after a relatively long delay time of 25 ps (relative to the cavity lifetime, which is <5 ps), the resultant excited-state population can be manipulated via the excitation frequency (polariton vs. dark-state excitation) or angle (the relative photon-vibration character of the polariton), which may prove useful in future implementation of cavity-modified molecular excitations.

Origin of 2D IR Spectra of Vibrational Polaritons: Deviations from the Free-Harmonic Boson. Even though we have shown that 2D IR spectra reveal dark states and their interactions with polaritons, the origin of the 2D IR spectra of vibrational polaritons is an interesting topic in its own right. Given previous emphasis on their linear response, polaritons have been primarily described within the free-boson picture, featuring harmonic oscillator dynamics (21, 30, 31). However, it is well-known that harmonic systems exhibit vanishing nonlinear optical response (32). Thus, the observation of vibrational-polariton pump–probe (16) and 2D IR signals necessarily indicates that this free-bosonic picture does not generally hold, and that anharmonicities in the system

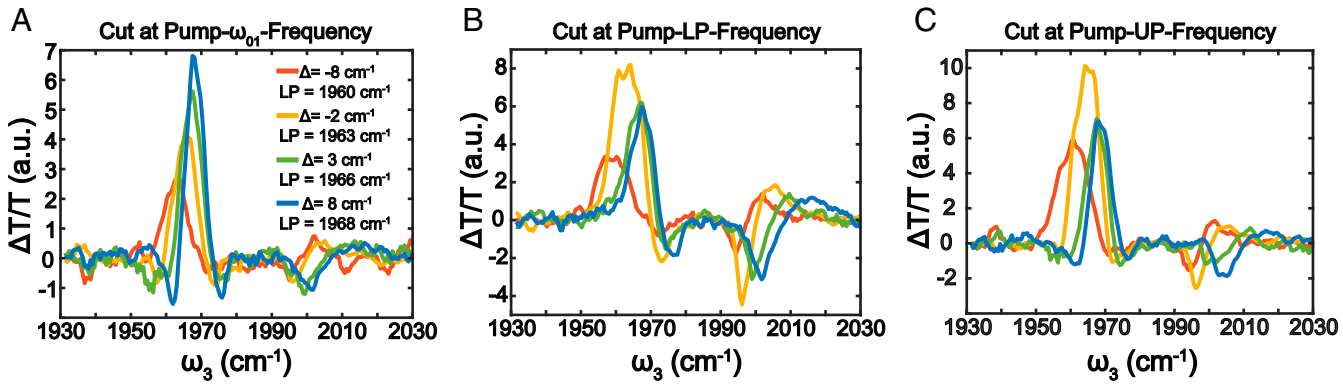

Fig. 4. Scaled spectral cuts at pump frequency of (*A*) ω_{01}, (*B*) LP, and (*C*) UP with different detuning (Δ).

must exist to give rise to nonlinear spectra. In inorganic semiconductor exciton–polaritons, effective anharmonicities are induced by Coulomb scattering and the so-called phase-space filling mechanism due to Pauli exclusion of electrons and holes (21, 33). For vibrations, nuclear and electrical (or dipolar) anharmonicity (34, 35) of the C–O stretch causes deviations from harmonic behavior. As the level of excitation in the system increases, v = 1–2 transitions become coupled to the cavity, in addition to the fundamental transition, thus influencing polariton formation and dispersion. Both the redshift of ω_{12} compared with ω_{01} (nuclear anharmonicity) and the reduced oscillator strength μ_{12} compared with $\sqrt{2}\mu_{01}$ (electrical anharmonicity) lead to a redshift of the UP (i.e., contraction of the vacuum Rabi splitting leading to derivative-like lineshape; *SI Appendix*, section 2e). Classical expressions for transmission through a cavity capture this effect well with respect to coupled reservoir population, but here we develop a full quantum-mechanical treatment to provide a microscopic perspective and shed light on the conditions of validity of the classical approximation.

The details of our approximate quantum-mechanical (QM) model are described in *SI Appendix*, section 4. The Hamiltonian includes the effects of both nuclear and electrical anharmonicity, which may be understood to induce self- and cross-interactions between the LP and UP, as well as between polaritons and dark states. With either the classical expression or the QM model, we can estimate the degree of coupled reservoir excitation by comparing the modeled and experimentally determined shift of the UP. From the classical model, we estimate that 5% of the molecules are excited at $t_2 = 25$ ps, while the QM model suggests 5–7.5%. Both estimates are reasonable for the pulse energies used. The QM model captures the main features of the vibrational-polariton (Fig. 5) pump–probe signal, including excited-state absorption, stimulated emission, and ground-state bleach, as well as the order of their corresponding intensities. We only present a comparison of experimental and theoretical pump–probe signals because simulation of the complete 2D spectrum requires a detailed theory of nonlinear multipolariton dynamics including many-body interactions between dark states and polaritons, which we are currently developing.

Discussion

While the assumption of transient reservoir-state population seems sufficient to capture several of the described 2D IR features (e.g., the derivative lineshape at UP and large absorptive feature at LP), the differences of 2D IR signals taken at ω_1 = LP, UP relative to those at $\omega_1 = \omega_{01}$ (Fig. 4) indicate that the time-dependent population of reservoir modes from polariton relaxation is surprisingly sensitive to cavity detuning. The quantum description presented here reproduces all of the characteristic features of the transient response at longer times, and a full treatment which includes the dynamic coherence and population transfer between polaritons and reservoir states is under development.

The multidimensional spectroscopy (36–40) of the cavity-coupled C–O stretch of $W(CO)_6$ reveals direct excitation of reservoir states (despite their weak linear response) and unambiguous evidence of interactions between reservoir and polariton modes. The visibility of reservoir dark-mode excitation in 2D IR signals arises from vibrational coherences that are detected through FID along t_1 of the emitted signal, instead of measuring the emitted optical responses, which can be weakened by reabsorption. The present work can be extended by performing polarization resolved measurements, quantum process tomography (41), or even 3D spectroscopy (42–44) for tracking emergent two-point correlations between vibrational polaritons and uncoupled vibrations. The integration between molecular vibrational transitions and quantized microcavity modes enables possibilities to design photonic materials in the mid-IR regimes, taking advantages of the large selection of vibrational transitions. Many novel molecular systems deserve attention, including heterogeneous systems, intrinsically coupled (34) and decoupled molecular vibrations, and molecular systems that undergo isomerization (45). In addition, many novel nanoplasmonic optics can be designed and used to enhance local electric field and hence the coupling strength (46).

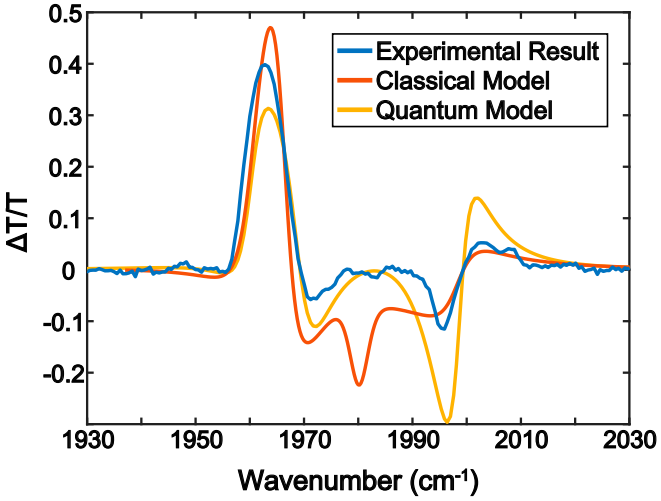

Fig. 5. Comparison between the experimental pump–probe signal and the classical and quantum models. Reasonable qualitative agreement is achieved.

Methods

Molecule–Polariton Preparation. The $W(CO)_6$ (Sigma-Aldrich)/cavity system is prepared in an IR spectral cell (Harrick) containing two dielectric CaF_2 mirrors separated by a 25-μm spacer and filled with nearly saturated $W(CO)_6$/hexane solution. The dielectric mirror has an ∼96% reflectivity. Because the Rabi splitting (37 cm^{-1}) is larger than the full width at half-maximum of both cavity (∼10 cm^{-1}) and $W(CO)_6$ vibrational (∼3 cm^{-1}) modes, the strong coupling criterion is satisfied. The transmission spectra of both pump and probe polaritons are measured along with 2D IR spectra.

Angular-Resolved 2D IR Spectrometer. The spectrometer follows the pulse-shaper-enabled pump–probe design (47), and a rotational stage is added to control beam incidence angle. In the 2D IR spectrometer, three IR pulses interact with a sample sequentially to create two vibrational coherences. The first coherence is characterized by scanning t_1. The second coherence introduces a macroscopic polarization which subsequently emits a third-order IR signal, which is self-heterodyned and detected in frequency domain. To display 2D IR spectra, the FID in t_1 is numerically Fourier transformed.

Theoretical Model. As described in *SI Appendix*, section 4, the QM model utilizes a Hamiltonian including a single-cavity mode interacting weakly with external vacuum electromagnetic modes, and with the polarization generated by N independent anharmonic molecular vibrations, which are themselves weakly coupled to low-energy bath modes. We utilize input-output theory to estimate the probe transmission in the presence and absence of a transient excited-state population of molecular vibrations.

ACKNOWLEDGMENTS. B.X., J.W., Y.L., and W.X. are supported by Air Force Office of Scientific Research Young Investigator Program Award, FA9550-17-1-0094 and by the Defense Advanced Research Projects Agency Young Faculty Award program, D15AP00107. B.S.S., A.D.D., and J.C.O. are supported by the Office of Naval Research through the Institute for Nanoscience at the Naval Research Laboratory. J.Y.-Z. and R.F.R. acknowledge support from NSF CAREER Award CHE:1654732 and generous University of California, San Diego (UCSD) startup funds. B.X. acknowledges the Roger Tsien Fellowship from the UCSD Department of Chemistry and Biochemistry.

1. Long JP, Simpkins BS (2015) Coherent coupling between a molecular vibration and Fabry–Perot optical cavity to give hybridized states in the strong coupling limit. *ACS Photonics* 2:130–136.
2. Shalabney A, et al. (2015) Coherent coupling of molecular resonators with a microcavity mode. *Nat Commun* 6:5981.
3. Ebbesen TW (2016) Hybrid light-matter states in a molecular and material science perspective. *Acc Chem Res* 49:2403–2412.
4. Amo A, et al. (2009) Superfluidity of polaritons in semiconductor microcavities. *Nat Phys* 5:805–810.
5. Kéna-Cohen S, Forrest SR (2010) Room-temperature polariton lasing in an organic single-crystal microcavity. *Nat Photonics* 4:371–375.
6. Plumhof JD, Stöferle T, Mai L, Scherf U, Mahrt RF (2014) Room-temperature Bose-Einstein condensation of cavity exciton-polaritons in a polymer. *Nat Mater* 13: 247–252.
7. Deng H, Haug H, Yamamoto Y (2010) Exciton-polariton Bose-Einstein condensation. *Rev Mod Phys* 82:1489–1537.
8. Daskalakis KS, Maier SA, Murray R, Kéna-Cohen S (2014) Nonlinear interactions in an organic polariton condensate. *Nat Mater* 13:271–278.
9. Deng H, Weihs G, Santori C, Bloch J, Yamamoto Y (2002) Condensation of semiconductor microcavity exciton polaritons. *Science* 298:199–203.
10. Muallem M, Palatnik A, Nessim GD, Tischler YR (2016) Strong light-matter coupling and hybridization of molecular vibrations in a low-loss infrared microcavity. *J Phys Chem Lett* 7:2002–2008.
11. Shalabney A, et al. (2015) Enhanced Raman scattering from vibro-polariton hybrid states. *Angew Chem Int Ed Engl* 54:7971–7975.
12. Simpkins BS, et al. (2015) Spanning strong to weak normal mode coupling between vibrational and Fabry–Pérot cavity modes through tuning of vibrational absorption strength. *ACS Photonics* 2:1460–1467.
13. Saurabh P, Mukamel S (2016) Two-dimensional infrared spectroscopy of vibrational polaritons of molecules in an optical cavity. *J Chem Phys* 144:124115.
14. Flick J, Ruggenthaler M, Appel H, Rubio A (2017) Atoms and molecules in cavities, from weak to strong coupling in quantum-electrodynamics (QED) chemistry. *Proc Natl Acad Sci USA* 114:3026–3034.
15. Hutchison JA, Schwartz T, Genet C, Devaux E, Ebbesen TW (2012) Modifying chemical landscapes by coupling to vacuum fields. *Angew Chem Int Ed Engl* 51:1592–1596.
16. Dunkelberger AD, Spann BT, Fears KP, Simpkins BS, Owrutsky JC (2016) Modified relaxation dynamics and coherent energy exchange in coupled vibration-cavity polaritons. *Nat Commun* 7:13504.
17. Houdré R, Stanley RP, Ilegems M (1996) Vacuum-field Rabi splitting in the presence of inhomogeneous broadening: Resolution of a homogeneous linewidth in an inhomogeneously broadened system. *Phys Rev A* 53:2711–2715.
18. Lindberg M, Binder R (1995) Dark states in coherent semiconductor spectroscopy. *Phys Rev Lett* 75:1403–1406.
19. Cho M (2008) Coherent two-dimensional optical spectroscopy. *Chem Rev* 108: 1331–1418.
20. Vasa P, et al. (2013) Real-time observation of ultrafast Rabi oscillations between excitons and plasmons in metal nanostructures with J-aggregates. *Nat Photonics* 7: 128–132.
21. Takemura N, et al. (2015) Two-dimensional Fourier transform spectroscopy of exciton-polaritons and their interactions. *Phys Rev B* 92:125415.
22. Arrivo SM, Dougherty TP, Grubbs WT, Heilweil EJ (1995) Ultrafast infrared spectroscopy of vibrational CO-stretch up-pumping and relaxation dynamics of W(CO)6. *Chem Phys Lett* 235:247–254.
23. Tokmakoff A, Sauter B, Kwok AS, Fayer MD (1994) Phonon-induced scattering between vibrations and multiphoton vibrational up-pumping in liquid solution. *Chem Phys Lett* 221:412–418.
24. Wen P, Christmann G, Baumberg JJ, Nelson KA (2013) Influence of multi-exciton correlations on nonlinear polariton dynamics in semiconductor microcavities. *New J Phys* 15:025005.
25. Gonzalez-Ballestero C, Feist J, Gonzalo Badía E, Moreno E, Garcia-Vidal FJ (2016) Uncoupled dark states can inherit polaritonic properties. *Phys Rev Lett* 117:156402.
26. Del Pino J, Feist J, Garcia-Vidal FJ (2015) Quantum theory of collective strong coupling of molecular vibrations with a microcavity mode. *New J Phys* 17:53040.
27. Takemura N, et al. (2016) Coherent and incoherent aspects of polariton dynamics in semiconductor microcavities. *Phys Rev B* 94:195301.
28. Scherer JJ, Paul JB, O'Keefe A, Saykally RJ (1997) Cavity ringdown laser absorption spectroscopy: History, development, and application to pulsed molecular beams. *Chem Rev* 97:25–52.
29. O'Keefe A, Deacon DAG (1988) Cavity ring-down optical spectrometer for absorption measurements using pulsed laser sources. *Rev Sci Instrum* 59:2544–2551.
30. Koch SW, Kira M, Khitrova G, Gibbs HM (2006) Semiconductor excitons in new light. *Nat Mater* 5:523–531.
31. Tassone F, Yamamoto Y (1999) Exciton-exciton scattering dynamics in a semiconductor microcavity and stimulated scattering into polaritons. *Phys Rev B* 59: 10830–10842.
32. Mukamel S, Nagata Y (2011) Quantum field, interference, and entanglement effects in nonlinear optical spectroscopy. *Procedia Chem* 3:132–151.
33. Jin GR, Liu WM (2004) Collapses and revivals of exciton emission in a semiconductor microcavity: Detuning and phase-space filling effects. *Phys Rev A* 70:13803.
34. Khalil M, Demirdöven N, Tokmakoff A (2003) Coherent 2D IR spectroscopy: Molecular structure and dynamics in solution. *J Phys Chem A* 107:5258–5279.
35. Herzberg G (1991) *Molecular Spectra and Molecular Structure: Infrared and Raman Spectra of Polyatomic Molecules* (Krieger Pub Co, Malabar, FL).
36. Middleton CT, et al. (2012) Two-dimensional infrared spectroscopy reveals the complex behaviour of an amyloid fibril inhibitor. *Nat Chem* 4:355–360.
37. Rosenfeld DE, Gengeliczki Z, Smith BJ, Stack TDP, Fayer MD (2011) Structural dynamics of a catalytic monolayer probed by ultrafast 2D IR vibrational echoes. *Science* 334:634–639.
38. Xiong W, et al. (2009) Transient 2D IR spectroscopy of charge injection in dye-sensitized nanocrystalline thin films. *J Am Chem Soc* 131:18040–18041.
39. Ishizaki A, Fleming GR (2012) Quantum coherence in photosynthetic light harvesting. *Annu Rev Condens Matter Phys* 3:333–361.
40. Eaves JD, et al. (2005) Hydrogen bonds in liquid water are broken only fleetingly. *Proc Natl Acad Sci USA* 102:13019–13022.
41. Yuen-Zhou J, et al. (2014) Coherent exciton dynamics in supramolecular light-harvesting nanotubes revealed by ultrafast quantum process tomography. *ACS Nano* 8: 5527–5534.
42. Garrett-Roe S, Hamm P (2009) Purely absorptive three-dimensional infrared spectroscopy. *J Chem Phys* 130:164510.
43. Li H, Bristow AD, Siemens ME, Moody G, Cundiff ST (2013) Unraveling quantum pathways using optical 3D Fourier-transform spectroscopy. *Nat Commun* 4:1390.
44. Turner DB, Stone KW, Gundogdu K, Nelson KA (2009) Three-dimensional electronic spectroscopy of excitons in GaAs quantum wells. *J Chem Phys* 131:144510.
45. Anna JM, Ross MR, Kubarych KJ (2009) Dissecting enthalpic and entropic barriers to ultrafast equilibrium isomerization of a flexible molecule using 2DIR chemical exchange spectroscopy. *J Phys Chem A* 113:6544–6547.
46. Gandman A, Mackin R, Cohn B, Rubtsov IV, Chuntonov L (2017) Two-dimensional Fano lineshapes in ultrafast vibrational spectroscopy of thin molecular layers on plasmonic arrays. *J Phys Chem Lett* 8:3341–3346.
47. Shim S-H, Zanni MT (2009) How to turn your pump-probe instrument into a multidimensional spectrometer: 2D IR and Vis spectroscopies via pulse shaping. *Phys Chem Chem Phys* 11:748–761.